Ca(OH)2/CaO reversible reaction in a fluidized bed reactor for thermochemical heat storage

Pedro Pardo, Zoé Anxionnaz-Minvielle, Sylvie Rougé, Patrick Cognet, Michel Cabassud

$Ca(OH)_2/CaO$ reversible reaction in a fluidized bed reactor for thermochemical heat storage

P. Pardo [a], Z. Anxionnaz-Minvielle [a,*], S. Rougé [a], P. Cognet [b,c], M. Cabassud [b,c]

[a] *CEA-LITEN-LETh, 17 rue des Martyrs, F-38054 Grenoble Cedex 9, France*
[b] *Université de Toulouse, INPT, UPS, Laboratoire de Génie Chimique, 4, Allée Emile Monso, F-31432 Toulouse, France*
[c] *CNRS, Laboratoire de Génie Chimique, F-31432 Toulouse, France*

Abstract

Thermal energy storage (TES) is a key factor for increasing the efficiency of concentrated solar power plants. TES using a reversible chemical reaction appears to be a promising technology for high energy density thermal storage (100–500 kW h m^{-3}), at high temperature (up to 1000 °C) and during a long period (24 h to several months). This paper details an experimental study to carry out the reversible reaction $Ca(OH)_{2(s)} + \Delta H_r \iff CaO_{(s)} + H_2O_{(g)}$ in a fluidized bed (FB) reactor. The 4 μm $Ca(OH)_2$ powder fluidization has been performed with an appropriate proportion of inert easy-to-fluidize particles. Then, $Ca(OH)_2$ dehydration and CaO hydration have been implemented in a FB reactor and 50 cycles have been reached. The mean energy density obtained is 60 kW h m^{-3} solid_mixture which amounts to a promising energy density of 156 kW h m^{-3} $Ca(OH)_2$-bulk if the reactants and the easy-to-fluidize particles are separated. The results demonstrated the feasibility of the implementation of the $Ca(OH)_2/CaO$ thermochemical heat storage in a fluidized bed reactor.

Keywords: Fluidized bed; $Ca(OH)_2/CaO$ reversible reaction; Thermal energy storage; Thermochemical storage

1. Introduction

Concentrated solar power plant (CSP) converts solar energy into electricity and could provide continuous electricity by integrating thermal energy storage (TES) system at high temperature level (400–1000 °C). Three kinds of TES systems are known: the sensible TES, the latent TES and the thermochemical one (Gil et al., 2010; Medrano et al., 2010). The latter appears to be a promising technique to store thermal energy at high energy density (100–500 kW h m^{-3}), high temperature level (up to 1000 °C) and during a long period (24 h to several months) (Schaube et al., 2011).

A thermochemical TES system involves a reversible reaction: $A + \Delta H_r \iff B + C$. Three steps are implemented: the charging step, the storage step and the releasing step. The Fig. 1 shows the process flowsheet of a CSP using a thermochemical TES system.

During the heat charging step (Fig. 1a), the heat provided by the solar field is used to dissociate a chemical reactant (A) into several products (B and C) meaning that the reaction is endothermic. Then, the products B and C are stored in two different tanks at either ambient temperature (long-term storage) or charging step temperature (24 h

* Corresponding author. Tel.: +33 438 78 35 67; fax: +33 438 78 51 61.
E-mail addresses: pierre.pardo@cea.fr (P. Pardo), zoe.minvielle@cea.fr (Z. Anxionnaz-Minvielle), sylvie.rouge@cea.fr (S. Rougé), patrick.cognet@ensiacet.fr (P. Cognet), michel.cabassud@ensiacet.fr (M. Cabassud).

http://dx.doi.org/10.1016/j.solener.2014.06.010

Nomenclature

Abbreviations

CHPs	Chemical Heat Pump system
CSP	concentrated solar power plant
EFP	easy-to-fluidize particle
FB	fluidized bed
TES	thermal energy storage
XRD	X-ray diffraction

Latin symbols

Cp	specific heat (kJ kg^{-1} K^{-1})
d_p	mean particle diameter (μm)
D	column diameter (m)
D_v	energy density (kW h m^{-3})
E	stored energy (kW h)
F	flow rate (kg s$^{-1)}$
H	column height (m)
m	mass (kg)
M	molar mass (kg mol^{-1})
n	mol number (mol)
P	power (kW)
R	radius (m)
t	time (min)
T	temperature (°C)
u	superficial velocity (cm s^{-1})
V	volume (m^3)
X	conversion rate (−)
$\%w$	mass fraction (−)

Greek symbols

ΔH_r	reaction enthalpy (J mol$^{-1)}$
ΔP	pressure drop (bar)
ΔP_{max}	maximal pressure drop (bar)
ΔP^*	normalized pressure drop (−)

Subscripts

Al_2O_3	Al_2O_3
$Ca(OH)_2$	$Ca(OH)_2$
charging	related to the charging step
chemical	related to the chemical energy
H_2O	H_2O
i	initial
mf	minimal condition of fluidization
t	transport
reaction	related to the reaction time
storage	related to the storage step
w	related to the duration of the charging or discharging step

storage for instance). To release the heat, the products of the endothermic reaction (B and C) are mixed together and react to restore the initial product (A) according to an exothermic reaction: this is the heat releasing step (Fig. 1b). Additional heat exchangers are used to recover the heat energy between the process streams.

To develop an efficient, reliable and profitable thermochemical TES system, different criteria are required: the reversibility of the reaction in an appropriate temperature range, the cycling stability, a high storage capacity, low cost and safe chemical compounds and a fast enough kinetics so that the solar energy absorption and the heat release can be quickly carried out (Wentworth and Chen, 1976).

Currently, four types of reversible reactions used for TES are commonly investigated.

- The ammonia dissociation-synthesis system: $2NH_3 + \Delta H_r \Longleftrightarrow N_2 + 3H_2$ has been studied for four decades by the Australian National University (ANU) (Dunn et al., 2012). This system was chosen because of the availability and low cost of ammonia, and the well-understood synthesis of NH_3 from N_2 and H_2 via the "Haber–Bosh" process (Gil et al., 2010; Dunn et al., 2012). The first solar driven high pressure ammonia reactor (1 kW) was successfully tested in a closed loop system (Kreetz and Lovegrove, 1999). It lead to the building of a scaled-up prototype (15 kW) tested in a 20 m^2 dish system (Lovegrove et al., 2004). However this system has several drawbacks as the use of catalysts, the high operating pressures (80–200 bar), the uncompleted conversion of both forward and reverse reactions and the H_2 and N_2 storage (gas phase).
- The magnesium hydride system: $MgH_2 + \Delta H_r \Longleftrightarrow Mg + H_2$ has been studied by the Max Plank Institute for 20 years. Felderhoff and Bogdanović (2009) reviewed the different works based on this reaction for TES applications. The drawbacks of this system are the slow reaction kinetics, the high operating pressures (50–100 bar) and the H_2 storage after the dehydrogenation step (Harries et al., 2012).
- Regarding the metal oxide systems, up to now, most of the studies deal with thermogravimetric analysis and feasibility studies (Wong et al., 2010). Recently, a solar heated rotary kiln was set-up, the feasibility of the reduction–oxidation reaction $2Co_3O_4 + \Delta H_r \Longleftrightarrow 6CoO + O_2$ was studied and thirty cycles were reached (Neises et al., 2012). The decomposition of Co_3O_4 occurs at 900 °C in a nitrogen atmosphere. This temperature is too high for a TES application in a CSP, but fits solar tower plant applications.
- The calcium hydroxide system: $Ca(OH)_2 + \Delta H_r \Longleftrightarrow CaO + H_2O$ has been studied for four decades (Ervin, 1977; Garg et al., 1985) and more recently by two different institutes, the Department of Urban

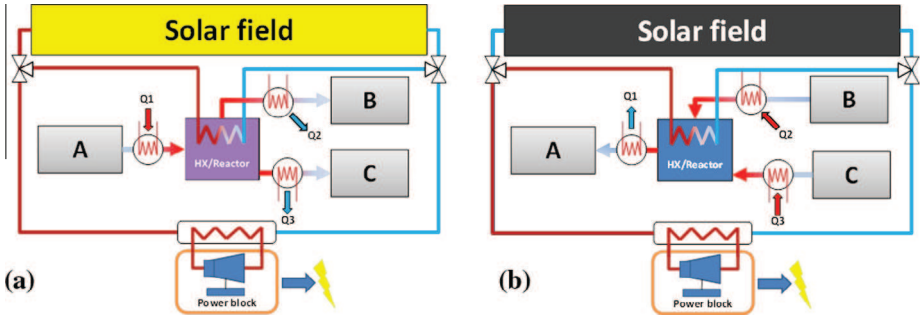

Fig. 1. Process flowsheet of a concentrated solar power plant using a thermochemical TES system: (a) heat charging step during the day and (b) heat releasing step during the night.

Environment Systems of Chiba University, as Chemical Heat Pump system (CHPs) (Ogura et al., 2003, 2004) and the German Aerospace Center (DLR) (Schaube et al., 2011, 2012a,b; Schmidt et al., 2014). This very promising system has many advantages as the high material volumetric energy density (195 kW h m^{-3} $Ca(OH)_2$-bulk), the good reversibility of the reaction (~100 cycles), appropriate operating temperatures and pressures (400–600 °C at 1 bar) (Schaube et al., 2012a), and the availability and non-toxicity of the reactants. That is the reasons why the $Ca(OH)_2$/CaO system was chosen for our study. However, this reversible reaction involves solid compounds and attention must be paid to their implementation to design an efficient storage process.

The objective of this work is to prove the feasibility of the $Ca(OH)_2$/CaO thermochemical TES system in a fluidized bed. Previous works, focused on the experimental approaches to carry out the gas–solid reversible reaction: $Ca(OH)_{2(s)} + \Delta H_r \Longleftrightarrow CaO_{(s)} + H_2O_{(g)}$ are reviewed. Then, the reactor technology choice is discussed and the fluidization behaviour of the calcium hydroxide powder is studied. Finally, the experimental results of both the high temperature implementation of $Ca(OH)_2$/CaO de/rehydration in a fluidized bed (FB) reactor and the cycling study are reported.

2. $Ca(OH)_2$/CaO state-of-the-art and reactor technology choice

The $Ca(OH)_2$/CaO de/rehydration has been theoretically and experimentally investigated by several authors for CSP application (Schaube et al., 2011; Brown et al., 1992; Werekobrobby, 1980), chemical heat pump (Fujimoto et al., 2002a,b; Ogura et al., 2003, 2004), preheating of engines (Darkwa, 1998) and power generation on the moon (Perez-Davis et al., 1992).

A chemical heat pump using $Ca(OH)_2$/CaO has been developed and modeled to study both high temperature storage and cold heat storage (Fujimoto et al., 2002a,b; Ogura et al., 2003, 2004). The amount of used CaO ranged from 200 g to 3 kg in a packed bed reactor.

Preliminary studies showed that the reaction rates (forward and backward reactions) are fast enough to use this reaction couple in a TES application (Ervin, 1977; Garg et al., 1985). The reversibility of the reaction was studied by Ervin (1977), Lin et al. (2009) and Schaube et al. (2012a,b). They respectively achieved 290 cycles, 20 cycles, and 100 cycles (ATG) – 25 cycles (fixed bed). These studies were made using a fixed bed reactor (~20 g (Ervin, 1977) – 60 g (Schaube et al., 2012b)) or a thermobalance (Schaube et al., 2012a; Lin et al., 2009). The kinetics of the forward and reverse reactions were studied by Matsuda et al. (1985) and Schaube et al. (2012a). Lin et al. (2006) studied the kinetics of the CaO hydration at high temperature (770 °C).

A TES system based on this reversible reaction could be technically and economically feasible for a CSP application (Schaube et al., 2011; Brown et al., 1992; Werekobrobby, 1980). The DLR is currently performing a study to use this reaction couple in a storage system (Schaube et al., 2011, 2012a,b). The works concern a thermogravimetric analysis, a reversibility analysis, a 2D numerical simulation and two experimental studies using a fixed bed reactor. Recently a 10 kW heat exchanger/reactor (20 kg of $Ca(OH)_2$) has been developed and tested (Schaube et al., 2012b; Schmidt et al., 2014).

To scale-up the storage process at pilot scale (1–10kW h), the reaction is implemented with few kg of solid compounds. As a consequence, moving beds have been considered to avoid high pressure drops and remove the heat and mass transfer barriers that could be met in large fixed bed. Four common technologies are listed:

- Fluidized bed (FB).
- Free fall bed.
- Rotary kiln.
- Screw extruder.

Rotary kiln and screw extruder are complex to operate because of the mechanical system for the reactor rotation. Moreover, a poor heat exchange between the particles and the reactor wall occurs (Kunii and Levenspiel, 1991). The previous kinetic studies showed that the reaction times of both $Ca(OH)_2$ dehydration and CaO hydration reactions

range between 1 and 30 min (Schaube et al., 2012a; Matsuda et al., 1985). In a free fall bed reactor the residence time is usually short, between 1 and 10 s (Villermaux, 1979). Thus, this technology is not suitable. As a consequence, the FB seems to be the most appropriate technology to perform the reversible reaction. Its advantages and drawbacks are listed in Table 1.

3. Experimental investigation

3.1. Part 1 – Fluidization behaviour of calcium hydroxide powder

Calcium hydroxide powder from ACRÔS ORGANICS with a median mean diameter of 3.8 μm, a true density of 2240 kg m^{-3} and a purity of 98% is used in this work. The particle diameter of commercial calcium hydroxide is generally close to 1–15 μm. Such particle diameter means that the powder is cohesive and belongs to group C of Geldart's classification, resulting in difficulties in achieving the fluidization (Geldart, 1973). Many solutions are reported in the literature to fluidize this kind of particles:

- Addition of inert easy-to-fluidize particles (EFP) (Alavi and Caussat, 2005).
- Addition of a fluidization additive (nanoparticles) (Saleh et al., 2006).
- Use of a mechanical agitation system (Alavi and Caussat, 2005).
- Use of a vibrated system (Alavi and Caussat, 2005).
- Shaping of the $Ca(OH)_2$ particles on a support (not presented in this work).

The easiest solution is to add inert EFP. It improves the fluidization, due to the mixing action of larger particles which can be assimilated to a mechanical agitator. $Ca(OH)_2$ and EFP solid mixtures were studied in a cold test section (see below) to assess the optimal fluidization conditions for our application and reach a bubbling or a turbulent fluidization. However this solution has some drawbacks:

- A separation unit is required downstream the reactor to have a high energy density during the storage step.
- Regarding the thermal efficiency of the whole storage process, the sensible thermal energy of the inert EFP must be recovered.

3.1.1. EFP material

The physical properties of the particles used in this work are listed in Table 2. The mean diameters were measured using a Malvern Mastersizer X, the bulk densities were experimentally assessed and the true density comes from literature data (Lide, 1991).

3.1.2. Experimental setup: cold test section

The experimental setup, described in Fig. 2, was designed to measure the pressure drops in the solid bed and to observe the solid bed behaviour during the fluidization.

The column is 0.7 m high, with a diameter of 0.08 m and is made of 5 mm thick Polymethyl Methacrylate (PMMA). The gas is distributed by 9 PMMA nozzles. Nitrogen used for the fluidization, is dried and compressed at 6 bar. Gas flow rate is controlled by a flow meter, Q_{gas} ($0–5 \pm 0.016$ Nm^3 h^{-1}). The type K thermocouple Te ($20–50 \pm 0.2$ °C) and the pressure transducer Pe ($1–2.5 \pm 0.008$ bar) measure respectively the inlet temperature and the inlet pressure of the gas. Two differential pressure transducers record pressure drops between the bottom and the top of the column, ΔP_{column} ($0–620 \pm 2.01$ mbar) and inside the bed, ΔP_{bed} ($0–400 \pm 2.30$ mbar). The transducers and the thermocouple of the experimental setup are connected to a data acquisition system unit AGILENT® HP 34970A.

3.1.3. Experimental procedure

For this experimental investigation, the ratio between the solid bed height and the column diameter equals 3. The pressure drops in the bed and the solid mixture behaviour have been studied during the increase and the decrease of the superficial gas velocity in the column. The experiments have been performed at ambient temperature and atmospheric pressure. The superficial gas velocity, u, ranges from 0 to 40 cm s^{-1} (±2.66%).

3.1.4. Results and discussion

Three solid mixture behaviours have been observed: gas channeling, fissure and bubbling fluidization as shown in Fig. 3.

To easily compare the different mixtures, the normalized pressure drop ΔP^*, defined in relation (1).

$$\Delta P^* = \Delta P(u)/\Delta P_{max} \quad (1)$$

Table 1
Advantages and drawbacks of FB reactor (Kunii and Levenspiel, 1991).

	Advantages	Drawbacks
Fluidized bed	– High heat transfer coefficient (100–600 W m^{-2} K^{-1}) – High mass transfer coefficient between the solid and the gas – Heat exchanger/reactor experience feedback – Forward and backward reactions in the same reactor – Homogenous temperatures – Well-known industrial scale-up	– Need of a fluidization gas – Particle attrition – Need of a separation unit – More expensive than a fixed bed reactor

Table 2
Physical properties of $Ca(OH)_2$ powder and the EFP used for $Ca(OH)_2$ fluidization.

Solid particles	d_p (μm)	Geldart Classification	True density (kg m^{-3})	Bulk density (kg m^{-3})
$Ca(OH)_2$	3.8	C	2200	490
CaO	3.8	C	3350	650
SiO_2–A	82.2	A	2196	1472
SiO_2–B	122.1	A	2196	1485
Al_2O_3–A	81.4	A	3970	815
Al_2O_3–B	171.7	A	3970	736
SiC–A	82.1	A	3160	1528
SiC–B	247.6	B	3160	1524

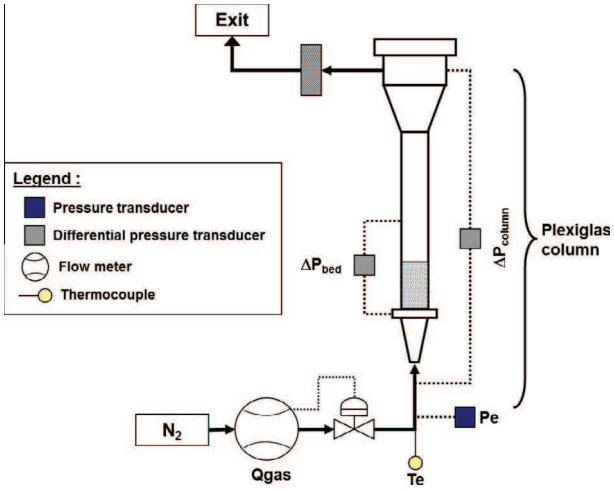

Fig. 2. Experimental setup, cold test section.

Fig. 4 shows the ΔP^* profiles of pure solids versus the superficial velocity. Solids belonging to both A and B groups of Geldart's classification show a ΔP^* profile characteristic of a fluidization activity. Below the minimal velocity of fluidization, ΔP^* increases with the superficial velocity. When the superficial velocity reaches the minimal velocity of fluidization, u_{mf}, ΔP^* becomes constant. Then, the bed expands with the increase of the superficial velocity. All these solids show bubbling or turbulent fluidization behaviour. On the other hand, as expected, the ΔP^* profile of $Ca(OH)_2$ powder, belonging to the C group of Geldart's classification, varies differently and never reaches a constant value. The observation of the test section actually shows that the fluidization did not occur because of the gas channelling.

To fluidize the $Ca(OH)_2$ powder, the fluidization behaviour of several solid mixtures containing various weight concentrations of inert EFP have been studied (see Table 3).

The same fluidization behaviour than with the pure $Ca(OH)_2$ powder is observed for the solid mixtures No. 1, 2, 3, 4, 6, 7 and 11 meaning that they also do not lead to a suitable fluidization.

Regarding the solid mixtures No. 8 and 9, ΔP^* does not vary continuously with the superficial velocity (see Fig. 5). At low superficial velocity, no bed expansion occurs and the pressure drop increases very quickly up to an inflexion point. By increasing again the superficial velocity, the bed expansion begins and the ΔP^* drops. Then, the bed expands again until the fluidization behaviour starts, characterized by a ΔP^* plateau. During the second part of the experiment, the superficial velocity decreases, the fluidization carries on and the ΔP^* is constant until the minimal superficial velocity of fluidization is reached. Then, the bed height decreases up to its initial value of 3 × diameter. This fluidization behaviour is also observed for the solid mixtures No. 5 and 10.

Thus, an appropriate amount of inert solid enables to fluidize the 4 μm $Ca(OH)_2$ powder. It can be noticed on Fig. 6 that if the Al_2O_3–B actually assists the $Ca(OH)_2$ fluidization, the interparticle forces remain strong as a high superficial velocity (10 cm s^{-1} versus 2 cm s^{-1} for pure particles of Al_2O_3–B) is required to obtain the minimal condition of fluidization.

In the following part of the work, the weight composition is the No. 9 mixture one: 70%wAl_2O_3–B/30%w$Ca(OH)_2$. Mixtures No. 5, 8 and 12 could also fit the criteria but No.

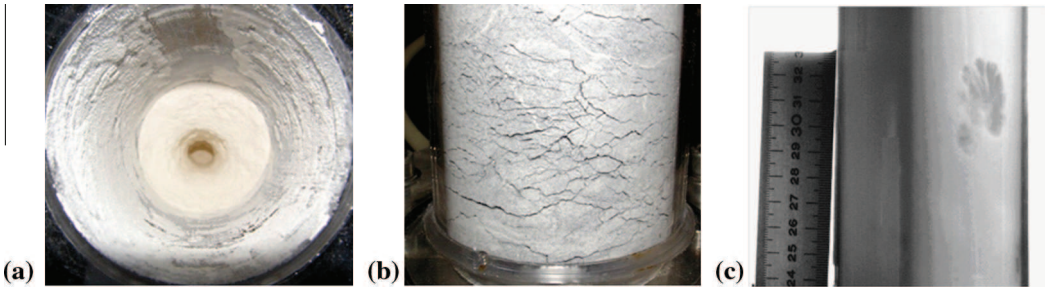

Fig. 3. Solid mixture behaviour (a) gas channelling, (b) fissure, and (c) bubbling fluidization.

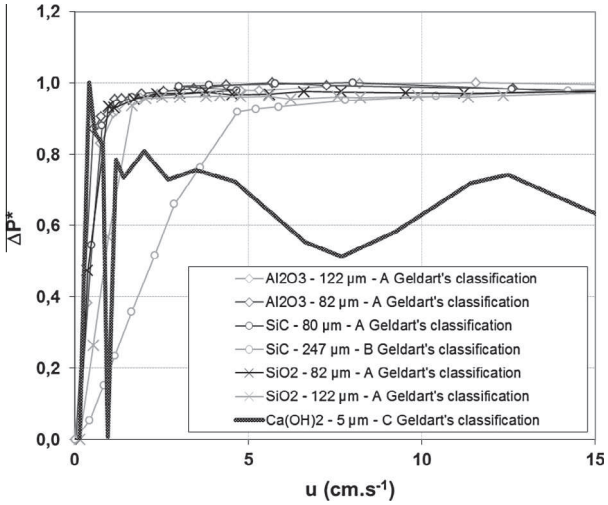

Fig. 4. ΔP^* profile versus superficial velocity for the pure solids listed in Table 2.

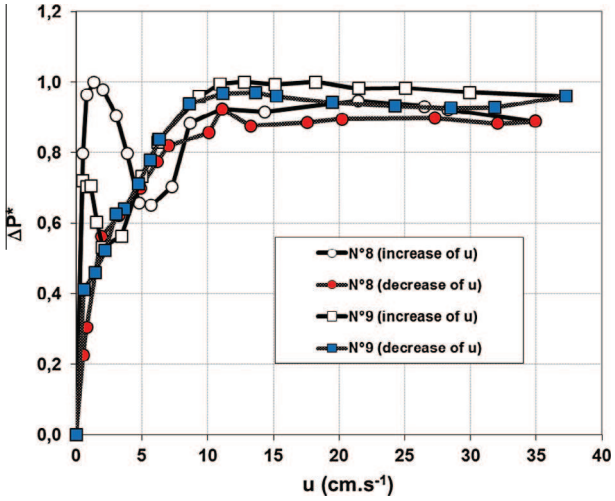

Fig. 5. ΔP^* profile of the solid mixtures No. 8: 65%$w$$Al_2O_3$–B/35%$w$$Ca(OH)_2$ and No. 9: 70%$w$$Al_2O_3$–B/30%$w$$Ca(OH)_2$.

9 is preferred because a more homogeneous fluidization has been observed.

The feasibility of the use of $Ca(OH)_2$ in a FB reactor thanks to the preliminary studies performed in the cold test section has been proven. The next step investigates the $Ca(OH)_2$ dehydration and the CaO hydration in real conditions of temperature and pressure in a hot test section.

3.2. Part 2 – $Ca(OH)_2$ dehydration, CaO hydration and cycling study in a fluidized bed reactor

3.2.1. Experimental setup: hot test section

The experimental setup, described in Fig. 7, was designed to assess the conversion rate of both $Ca(OH)_2$ dehydration and CaO hydration reactions in a FB reactor. The process is performed in batch conditions. Up to 3 kg of solid can be introduced into the reactor. The hot reactor is designed to operate at 550 °C and 2 bar. It is made of 11 mm thick stainless steel 316L. The column is 1.4 m high, connected with a 0.15 m high cone. The column diameter is 0.114 m. The gas distribution is achieved through 21 nozzles. A porous plate filter (<10 µm) is located in the head of the test section to prevent the fine solid particles from going out. An electrical 5.5 kW resistance fixed to the outlet shell is used to heat the test section until 550 °C. To minimize the heat losses to the ambient, 200 mm thick isolation layers enclose the column (0.04 W m^{-1} K^{-1} thermal conductivity).

13 Thermocouples Type K of 1 mm (25–550 ± 0.2 °C) are used in the test section. The bed is equipped with 6 thermocouples in order to measure the temperature within the reactor. Table 4 lists the positions of each test section thermocouple. The thermocouple T_w is used to regulate the wall temperature of the reactor. It is fixed to the outlet shell. Two additional thermocouples, $T4$ and $T5$, record respectively the inlet and the outlet temperatures of the column. $T3$ and $T6$ record the temperatures close to the hygrometer sensors $H1$, $H2$ and $H3$. Two pressure transducers, $P1$ (1–2.5 ± 0.008 bar) and $P2$ (1–2.5 ±

Table 3
Experimental investigation of the solid mixtures.

No.	Solid mixture		Maximal pressure drop ΔP_{max} (mbar)	Solid mixture behaviour
	%w EFP	%w $Ca(OH)_2$		
0	0%wEFP	100%$w$$Ca(OH)_2$	11.4	Gas channelling
1	70%$w$$SiO_2$–A	30%$w$$Ca(OH)_2$	11.9	Gas channelling
2	80%$w$$SiO_2$–A	20%$w$$Ca(OH)_2$	16.1	Gas channelling
3	60%$w$$SiO_2$–B/	40%$w$$Ca(OH)_2$	14.6	Gas channelling
4	70%$w$$SiO_2$–B	30%$w$$Ca(OH)_2$	13.3	Gas channelling
5	80%$w$$SiO_2$–B	20%$w$$Ca(OH)_2$	16.3	Bubbling/turbulent fluidization
6	60%$w$$Al_2O_3$–A	40%$w$$Ca(OH)_2$	11.7	Gas channelling
7	70%$w$$Al_2O_3$–A	30%$w$$Ca(OH)_2$	12.9	Gas channelling
8	65%$w$$Al_2O_3$–B	35%$w$$Ca(OH)_2$	11.0	Bubbling/Turbulent fluidization
9	70%$w$$Al_2O_3$–B	30%$w$$Ca(OH)_2$	11.3	Bubbling/Turbulent fluidization
10	80%$w$$Al_2O_3$–B	20%$w$$Ca(OH)_2$	12.9	Bubbling/Turbulent fluidization
11	80%wSiC–A	20%$w$$Ca(OH)_2$	13.4	Cracks and gas channelling
12	80%wSiC–B	20%$w$$Ca(OH)_2$	13.9	Bubbling/Turbulent fluidization

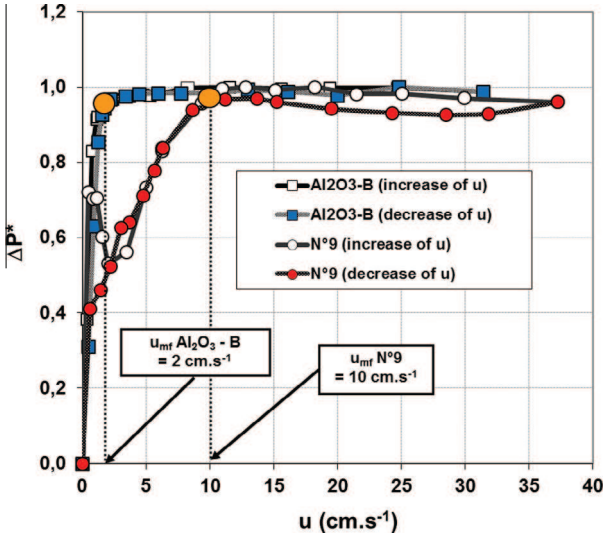

Fig. 6. ΔP^* profiles of the solid mixture No. 9: 70%$w$$Al_2O_3$–B/30%$w$$Ca(OH)_2$ and pure Al_2O_3–B.

0.009 bar), measure respectively the pressure at the hygrometer sensor $H1$ and at the inlet of the column. Two differential pressure transducers are used to assess the pressure drop of the column, ΔP_{column} (0–400 ± 2.30 mbar) and between the bottom of the column and the hygrometer sensor $H2$, ΔP_{filter} (0–620 ± 2.01 mbar). Two flow meters, Q_{water} (mini Cori-flow BRONKHORST) and Q_{gas} (BROOKS 5853S), record inlet flow rates of both tap water (0–5 ± 0.012 kg h^{-1}) and compressed nitrogen system (0–5 ± 0.016 Nm^3 h^{-1}). The water evaporation and the gas mixing are done in a 6 kW vapour generator where the gas mixture outlet temperature is regulated at 220 °C. Finally, two capacitive hygrometers HC2-HC102 from ROTRONIC (0–100 ± 2.39%HR, 20–200 ± 0.2 °C), $H1$ and $H2$, are

Table 4
Thermocouple location into the test section.

Thermocouple	Location
TSE1	$H = 40$ mm – $r/R = 1$
TSE2	$H = 140$ mm – $r/R = 1$
TSE3	$H = 240$ mm – $r/R = 1$
TSE4	$H = 340$ mm – $r/R = 1$
TSE5	$H = 240$ mm – $r/R = 1/3$
TSE6	$H = 240$ mm – $r/R = 2/3$
T_w	$H = 240$ mm – $r/R = 0$

respectively used to assess the inlet and outlet water flow rates. The sensors, the transducers and the thermocouples of the experimental setup are connected to a data acquisition system unit AGILENT® HP 34970A. To minimize the heat losses to the ambient, 100 mm thick isolation layers enclose all the gas streams (0.04 W m^{-1} K^{-1} thermal conductivity).

3.2.2. Experimental procedure

To perform the experiments, a 1.93 kg mixture of 70%$w$$Al_2O_3$–B and 30%$w$$Ca(OH)_2$ has been used. The solid bed height is equal to 3 diameters.

3.2.2.1. Fluidization behaviour. First of all, the fluidization behaviour in the hot test section wa investigated at 25 °C and 300 °C. The procedure of Section 3.1.3 was applied. Fig. 8 shows the ΔP^* profiles of the solid mixture No. 9: 70%$w$$Al_2O_3$–B/30%$w$$Ca(OH)_2$ versus the superficial velocity at 25 and 300 °C. The maximal pressure drop, ΔP_{max}, is equal to 21.6 mbar. A minimal superficial velocity of 6 ± 0.5 cm s^{-1} has been measured for both temperatures. This value is lower than the cold test section one. The reactor material of both test sections may be involved. Indeed, the cold test section is made of PMMA which generates

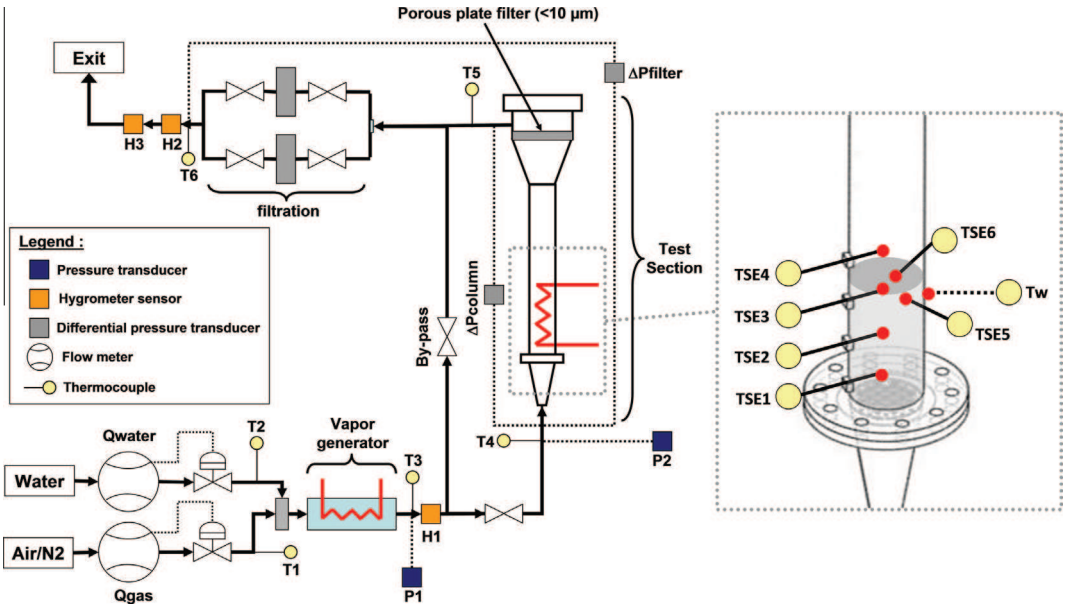

Fig. 7. Experimental setup, hot test section.

more electrostatic forces than the stainless steel 316L wall of the hot test section. Furthermore, the section diameters are different, it could also change the interaction forces between the wall and the solid.

3.2.2.2. Reactions and cycling study. First of all, the wall test section is slowly heated with a temperature ramp of 250 °C h^{-1} from 25 °C to 330 °C, temperature at which the dehydration does not occur. Nitrogen flow is set at 2 Nm^3 h^{-1} and its temperature is 300 °C whereas the inlet liquid water flow is 0 kg h^{-1}, meaning an inlet water partial pressure of 0 kPa. To perform the dehydration reaction, the wall of the reactor is heated with a fast temperature ramp (30 °C min^{-1}) up to 480 °C and this temperature is then kept constant (regulated by *Tw*). During the reaction, filter cleaning is required to remove the caked-on powder from the filter. To perform this operation, the test section is by-passed and the valves upstream the hygrometer sensor *H*2 are closed. As a consequence, a back-pressure appears at the top of the column and the by-passed gas removes the caked-on powder. Then, the valves before the hygrometer sensor *H*2 are opened and the by-pass is closed to let the gas mixture flowing through the reactor. The end of the reaction is reached when both the inlet and the outlet water flow rates are equal (0 kg h^{-1}).

After this reaction an Al_2O_3/CaO solid mixture remains in the reactor. To perform the hydration reaction, the wall temperature T_w is set at 350 °C. The test section is then by-passed. The inlet nitrogen flow rate and the water flow rate are respectively set at 2 Nm^3 h^{-1} and 0.49 kg h^{-1}, meaning an inlet water partial pressure of 31.1 kPa which corresponds to an equilibrium temperature of 455 °C. The inlet gas mixture temperature is regulated at 300 °C. When both the inlet and outlet water flow rates are equal and the temperature is at steady state, the by-pass is closed to let the gas mixture flowing through the reactor. Thus, the hydration reaction starts. The thermal energy released by the exothermic reaction is not recovered in this simplified system. It is removed by the heat losses to the ambient. The hydration reaction is finished when both the inlet and outlet water flow rates are equal (0.49 kg h^{-1}). Then, the wall temperature T_w is fixed to 330 °C. The test section is cooled with the heat losses to the ambient. Then, the procedure starts again to perform the dehydration reaction. Three de/rehydration cycles can be performed within 10 h.

3.2.3. Experimental results

3.2.3.1. $Ca(OH)_2$ dehydration reaction. Fig. 9 shows the temperature profiles in the FB reactor and the wall temperature during the $Ca(OH)_2$ dehydration. Since the temperature profiles inside the FB reactor (*TSE*1–*TSE*6) are all together, it can be concluded that the reactor allows perfectly homogeneous temperatures. As the dehydration is an endothermic reaction, the solid mixture temperature is lower than the wall temperature and the power flux is transferred from the wall towards the solid mixture.

Fig. 10 shows both inlet and outlet H_2O flow rates during the dehydration reaction. The inlet water partial pressure is 0 kPa, with a total pressure in the system of 133 kPa. When the solid mixture temperature reaches 330 °C (see Fig. 9) the dehydration reaction starts. This is characterized by a release of water ($t = 119$ min). During the temperature ramp, the outlet H_2O flow rate increases up to a maximum value of 0.33 kg h^{-1} corresponding to the wall temperature of 480 °C. Then, the wall temperature stays constant (±2 °C) and the outlet H_2O flow rate decreases slowly until reaching 0 kg h^{-1}. Two filter cleanings are done during the dehydration reaction, at $t = 151$ min and $t = 158$ min, to remove the caked-on powder from the filter. After each filter cleaning step, the accumulated powder in the top of the test section falls down into the bed reactor to react. In this test, the reaction

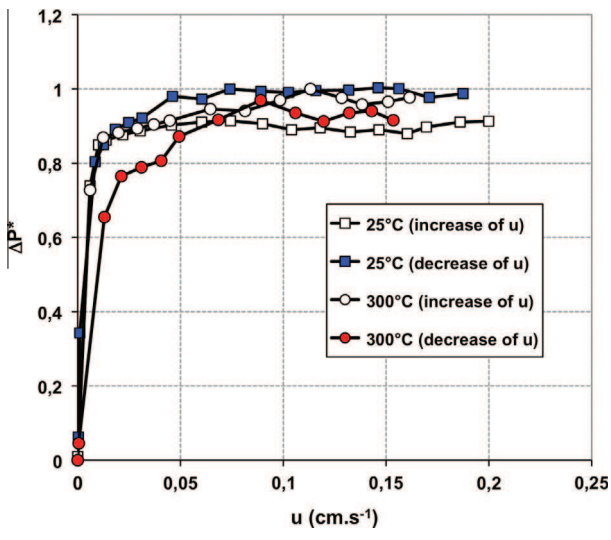

Fig. 8. ΔP^* profiles of the solid mixture No. 9: 70%*w*Al_2O_3–B/30%*w*$Ca(OH)_2$ in the hot test section at 25 and 300 °C.

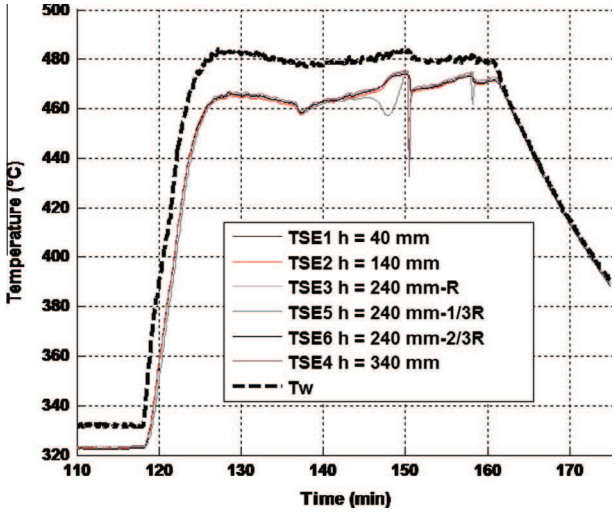

Fig. 9. Temperature profiles in the fluidized bed reactor during $Ca(OH)_2$ dehydration reaction with nitrogen and water inlet flow rates of 2 Nm^3 h^{-1} and 0 kg h^{-1} respectively.

is carried out between 119 and 170 min. The total conversion rate of the calcium hydroxide is 90% (±5.52%) after 51 min.

3.2.3.2. CaO hydration reaction. Fig. 11 shows the temperature profiles inside the FB reactor and the wall temperature during the CaO hydration reaction. As the hydration is an exothermic reaction, the solid mixture temperature is higher than the wall temperature and the heat is transferred from the solid mixture to the wall. There is an increase of the bed temperature during the experimental test from 345 to 385 °C because the heat generated by the reaction is just removed by the thermal losses of the apparatus to the ambient. These heat losses are not high enough to cool the reactor so as to keep the bed temperature constant.

Fig. 12 shows both the inlet and outlet H_2O flow rates during the CaO hydration reaction. The reaction starts at $t = 203$ min and is characterized by a water consumption. The inlet water partial pressure is 31.1 kPa, with a total pressure in the system of 134 kPa. At the beginning of the reaction, the outlet water flow rate drops quickly to 0.01 kg h^{-1} with an increase of the bed temperature (see Fig. 11). Then, the water consumption decreases slowly and stops at $t = 230$ min when both the inlet and outlet water flow rates are equal (0.49 kg h^{-1}). In this test, the reaction is carried out between 204 and 232 min. The total conversion rate of the calcium oxide is 99% (±4.19%) after 28 min.

3.2.3.3. Cycling study. To have an efficient thermochemical TES system, the reversibility of the reaction must remain constant all along the cycles. A cycle is defined as the dehydration reaction followed by the hydration reaction. To perform the cycling study, the procedure of Section 3.2.2

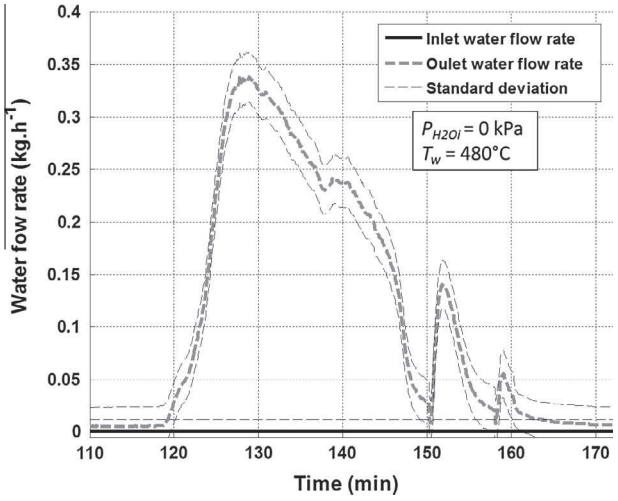

Fig. 10. Water flow rates during $Ca(OH)_2$ dehydration reaction with nitrogen and water inlet flow rates of 2 Nm^3 h^{-1} and 0 kg h^{-1} respectively and wall reactor temperature (Tw) of 480 °C.

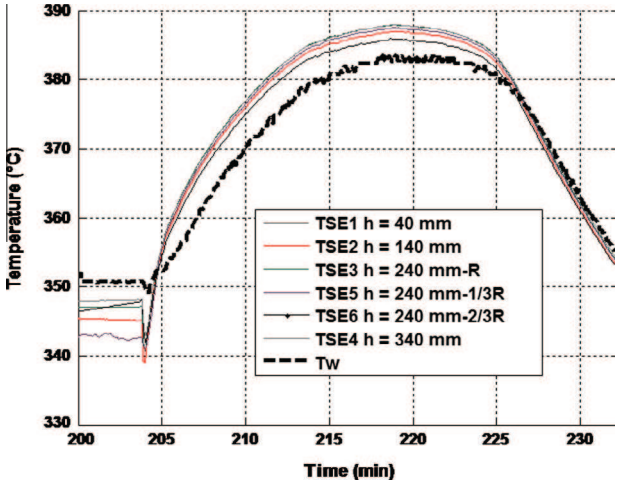

Fig. 11. Temperature profiles in the fluidized bed reactor during CaO hydration reaction with nitrogen and water inlet flow rates of 2 Nm^3 h^{-1} and 0.49 kg h^{-1} respectively.

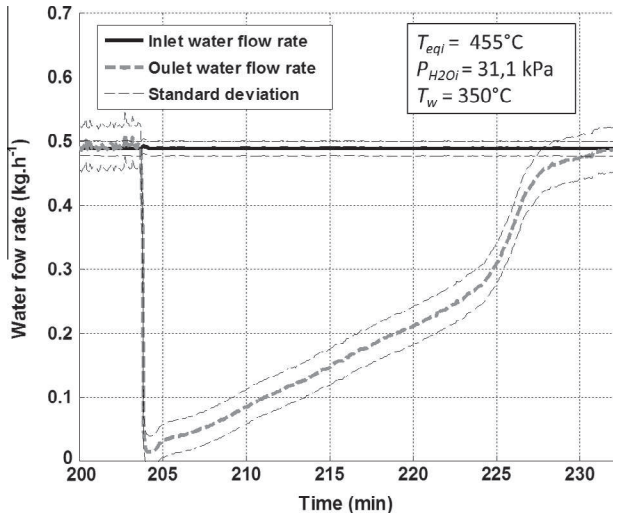

Fig. 12. Water flow rates during CaO hydration reaction with nitrogen and water inlet flow rates of 2 Nm^3 h^{-1} and 0.49 kg h^{-1} respectively and initial wall reactor temperature (Tw) of 350 °C.

has been applied and the final conversion rate of each reaction has been assessed according to the relation (2).

$$X = n_{H_2O}/n_{Ca(OH)2i} \quad (2)$$

Fig. 13 shows the conversion rates profile of both dehydration and hydration reactions during the cycling study.

The conversion rates decrease from 0.9 to 0.7 during the first 17th cycles. Between the 17th and the 18th cycle, the reactor has been opened to remove the accumulated particles located at the top larger section of the fluidized bed and to put them back in the fluidized reaction zone. This operation has also been carried out before the cycles 32 and 44. After these cleaning steps, the conversion rates of both reactions go up again close to their initial values, i.e. 0.9. This observation means that, as the cycle number increases, part of the reactive particles is taken away

towards the top of the reactor where the gas velocity is low and cannot react. To prevent this phenomenon, a cyclone and a circulation system used to recover the particles in the reactor must be set up into the hot test section. XRD analyses of both pure and cycled products have been made. Fig. 14 shows the diffraction diagrams of the cycled sample compared to the references ($Ca(OH)_2$, Al_2O_3).

After 50 cycles, any secondary product has been formed. It can be concluded that the reaction stability is not affected by the use of both Al_2O_3 and nitrogen. The $Ca(OH)_2/CaO$ couple can, thus, be used for a TES application in a fluidized bed without loss of material as the number of cycles increases.

3.2.4. Discussion

To perform the $Ca(OH)_2$ fluidization, an important quantity of Al_2O_3 EFP has been used (70%*w*). It has two major drawbacks: energy densities will be drastically reduced and the sensible heat of Al_2O_3 will represent an important part of the stored heat. The Al_2O_3 EFP must be separated and recycled in the reactor after each step. A simplified flowsheet of a continuous thermochemical energy storage process using a FB reactor with EFP is illustrated in Fig. 15.

Al_2O_3 separation is required to keep the energy density as high as possible. Industrial methods are used to separate solid/solid mixtures. Among these techniques, a sieving or a cyclone unit located downstream the reactor could perform our solid separation. The discrepancy of the particles diameters between the EFP particles and the CaO/$Ca(OH)_2$ powder makes easier this separation. However these additional unit operations will involve an increase of energy consumption that has not been assessed yet.

The mean conversion rate obtained during the cycling study is 80%. The mean energy density reached in the reactor during the cycling study can be calculated with the relation (3):

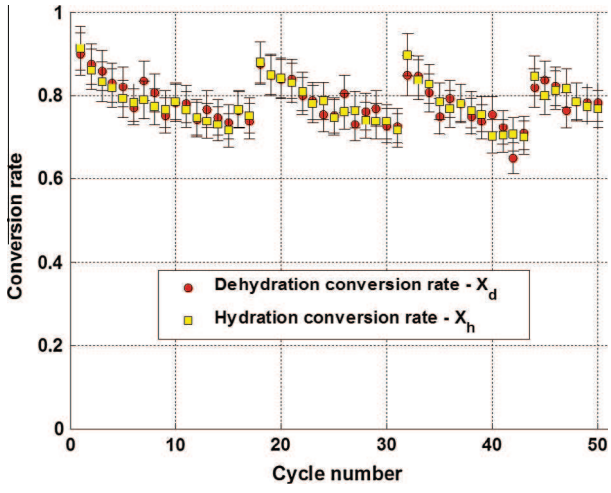

Fig. 13. Conversion rate of both reactions during the cycling study; dehydration: $T_w = 480\ °C$ – $Q_{N2} = 2\ Nm^3\ h^{-1}$ – $Q_{water} = 0\ kg\ h^{-1}$; hydration: $T_w = 480\ °C$ – $Q_{N2} = 2\ Nm^3\ h^{-1}$ – $Q_{water} = 0.49\ kg\ h^{-1}$.

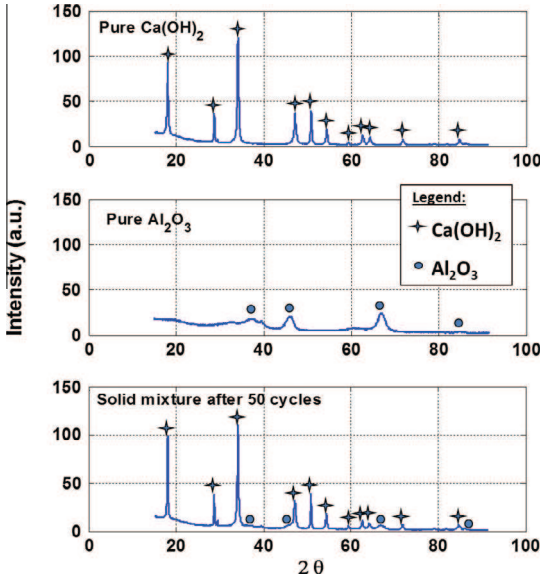

Fig. 14. Diffratograms of pure $Ca(OH)_2$, pure Al_2O_3 and 70%*w*Al_2O_3 and 30%*w*$Ca(OH)_2$ mixture after 50 cycles.

$$D_v = (n_{Ca(OH)2i} \times X_d \times (\Delta H_r/3600))/(V_{Ca(OH)_2} + V_{Al_2O_3}) \quad (3)$$

The energy density assessed in our fluidized bed is 60 kW h m^{-3} $Ca(OH)_2/Al_2O_3$. If the solid separation operation is done after the reaction step, the energy density of 156 kW h m^{-3} $Ca(OH)_2$-bulk is reached.

Al_2O_3 recycling stream from the solid/solid separation unit to the reactor will allow the reduction of EFP quantity to perform the process. It will consequently reduce the part of the stored Al_2O_3 sensible heat. It is interesting to plot the energy ratio between the stored Al_2O_3 sensible heat and the stored thermochemical energy versus the operating time. In our reaction conditions, the limiting reaction is the dehydration one, with a reaction time of 51 min. For a fixed process power, the stored energy depends on the operating time, i.e. the duration of the charging or discharging step.

$$E_{chemical} = P \times t_w \quad (4)$$

The $Ca(OH)_2$ mass flow rate can be assessed through the relation (5)

$$F_{Ca(OH)_2} = P/(\Delta H_r \times M_{Ca(OH)_2}) \quad (5)$$

Then, the mass of Al_2O_3 required to perform the $Ca(OH)_2$ fluidization can be assessed through the relation (6).

$$m_{Al_2O_3} = F_{Ca(OH)_2} \times x_{Al_2O_3}/x_{Ca(OH)_2} \times t_{reaction} \quad (6)$$

Finally, the Al_2O_3 sensible heat stored in the process is obtained with the relation (7).

$$E_{Al_2O_3} = m_{Al_2O_3} \times Cp_{Al_2O_3} \times (T_{charging} - T_{storage}) \quad (7)$$

Fig. 16 shows the profile of the $E_{Al_2O_3}/E_{chemical}$ ratio versus the operating time for two storage temperatures.

Al_2O_3 sensible heat stored part is more important if the products are stored at ambient temperature (i.e.

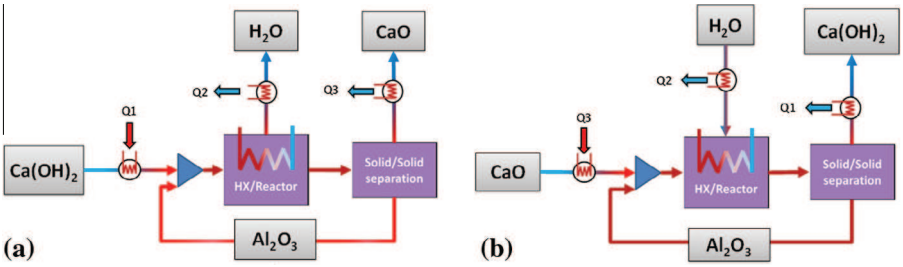

Fig. 15. Simplified flowsheet of continuous thermochemical energy storage process using a fluidized bed reactor with EFP: (a) charging step and (b) discharging step.

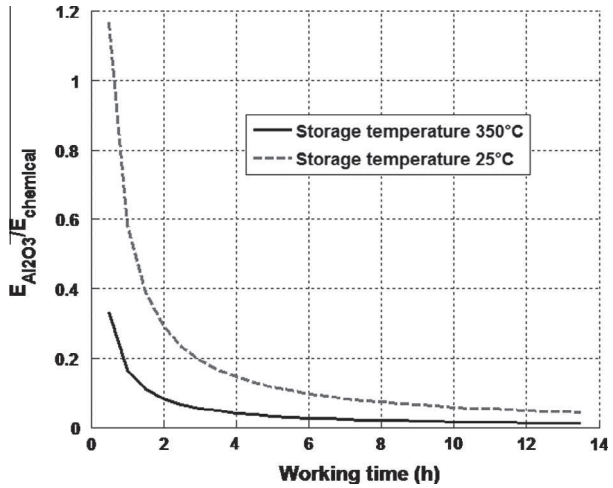

Fig. 16. $E_{Al_2O_3}/E_{chemical}$ ratio versus the operating time for two storage temperatures: 25 °C and 350 °C.

inter-seasonal storage) than a storage at working temperature, e.g. 350 °C (i.e. a daily storage). For both temperatures, above a charging period equal to 4 h, the Al_2O_3 sensible heat stored part is under 20% of the stored chemical energy. In summer, during a sunny day, the working time of a CSP can reach 4–8 h. Thus, this thermal storage system remains efficient with more than 80% of the heat stored by the thermochemical way above 4 h of charging period.

4. Conclusions

The $Ca(OH)_2$ powder fluidization and the reversible reaction $Ca(OH)_{2(s)} \iff CaO_{(s)} + H_2O_{(g)}$ have been experimentally investigated. To perform the fluidization of the 4 μm commercial $Ca(OH)_2$ powder, inert easy-to-fluidize particles have been used with the following weight concentration: 70%wAl_2O_3–B/30%$wCa(OH)_2$. A sample of 1.93 kg of this solid mixture has been implemented in a fluidized bed reactor to perform the $Ca(OH)_2$ dehydration reaction at 480 °C and the CaO hydration reaction at 350 °C. 50 cycles have been performed. It proves the feasibility of storing thermal energy with the $Ca(OH)_2$/CaO de/rehydration reactions in a fluidized bed. A mean energy density of 60 kW h m^{-3} $Ca(OH)_2$–Al_2O_3 has been reached in the reactor which amounts to a promising energy density of 156 kW h m^{-3} $Ca(OH)_2$-bulk once the reactant and the easy-to-fluidized particles are separated. Moreover, if the Al_2O_3 powder is recycled into the reactor its sensible heat represents less than 20% of the total stored heat assuming a minimal charging period equal to 4 h.

References

Alavi, S., Caussat, B., 2005. Experimental study on fluidization of micronic powders. Powder Technol. 157, 114–120.

Brown, D.R., La Marche, J.L., Spanner, G.E., 1992. Chemical Energy Storage System for SEGS Solar Thermal Power Plant. Report. Pacific Northwest Laboratory, Richland, USA.

Darkwa, K., 1998. Thermochemical energy storage in inorganic oxides: an experimental evaluation. Appl. Therm. Eng. 18 (6), 387–400.

Dunn, R., Lovegrove, K., Burgess, G., 2012. A review of ammonia-based thermochemical energy storage for concentrating solar power. Proc. IEEE 100 (2), 391–400.

Ervin, G., 1977. Solar heat storage using chemical reactions. J. Solid State Chem. 22, 51–61.

Felderhoff, M., Bogdanović, B., 2009. Review: high temperature metal hydrides as heat storage materials for solar and related applications. Int. J. Mol. Sci. 10, 325–344.

Fujimoto, S., Bilgen, E., Ogura, H., 2002a. CaO/$Ca(OH)_2$ chemical heat pump system. Energy Convers. Manage. 43, 947–960.

Fujimoto, S., Bilgen, E., Ogura, H., 2002b. Dynamic simulation of CaO/$Ca(OH)_2$ chemical heat pump systems. Exergy 2, 6–14.

Garg, H.P., Mullick, S.C., Bhargara, A.K., 1985. Solar Thermal Energy Storage. D. Reidel Publishing Company, Dordrecht, Holland.

Geldart, D., 1973. Types of gas fluidization. Powder Technol. 7 (5), 285–292.

Gil, A., Medrano, M., Martorell, I., Lazaro, A., Dolapo, P., Zalba, B., Cabeza, L.F., 2010. State of the art on high temperature thermal energy storage for power generation. Part 1 – Concepts, materials and modelisation. Sust. Energy Rev. 14 (1), 31–55.

Harries, D.N., Paskevicius, M., Shepard, D.A., Price, T.E.C., Buckley, C.E., 2012. Concentrated solar thermal heat storage using metal hydrides. Proc. IEEE 100 (2), 539–549.

Kreetz, H., Lovegrove, K., 1999. Theoretical analysis and experimental results of a 1 kW chem ammonia synthesis reactor for a solar thermochemical energy storage system. Sol. Energy 67, 287–296.

Kunii, D., Levenspiel, O., 1991. Fluidization Engineering, second ed. Butterworth-Heinemann, Boston.

Lide, D.R., 1991. CRC Handbook of Chemistry and Physics, 72nd ed.

Lin, S., Harada, M., Suzuki, Y., Hatano, H., 2006. CaO hydration rate at high temperature (~1023 K). Energy Fuels 20, 903–908.

Lin, S., Wang, Y., Suzuki, Y., 2009. High-temperature CaO hydration/$Ca(OH)_2$ decomposition over a multitude of cycles. Energy Fuels 23, 2855–2861.

Lovegrove, K., Luzzi, A., Soldiani, I., Kreetz, H., 2004. Developing ammonia based thermochemical energy storage for dish power plants. Sol. Energy 76, 331–337.

Matsuda, H., Ishizu, T., Lee, S.K., Hasatani, M., 1985. Kinetic study of $Ca(OH)_2$/CaO reversible thermochemical reaction for thermal energy

storage by means of chemical reaction. Kagaku Kogaku Ronbunshu 11, 542–548.
Medrano, M., Gil, A., Martorell, I., Potau, X., Cabeza, L.F., 2010. State of the art on high-temperature thermal energy storage for power generation. Part 2 – Case studies. Renew. Sust. Energy Rev. 14 (1), 56–72.
Neises, M., Tescari, S., De Oliveira, L., Roeb, M., Sattler, C., Wong, B., 2012. Solar-heated rotary kiln for thermochemical energy storage. Sol. Energy 86, 3040–3048.
Ogura, H., Yamamoto, T., Kage, H., 2003. Efficiencies of $CaO/H_2O/Ca(OH)_2$ chemical heat pump for heat storing and heating cooling. Energy 23, 1479–1493.
Ogura, H., Abliz, S., Kage, H., 2004. Studies on applicability of scallop material to calcium oxide/calcium hydroxide chemical heat pump. Fuel Process. Technol. 85, 1259–1269.
Perez-Davis, M.E., McKissock, B.I., DiFilippo, F., 1992. Thermochemical energy storage for lunar base. NASA Technical Memorandum 105333.
Saleh, K., Cami, X.B., Thomas, A., Guigon, P., 2006. An experimental study on the fluidization behaviour of Geldart C class powders. KONA 24, 134–144.
Schaube, F., Wörner, A., Tamme, R., 2011. High temperature thermochemical heat storage for concentrated solar power plant using gas–solid reactions. J. Sol. Energy Eng. 133.
Schaube, F., Koch, L., Wörner, A., Müller-Steinhagen, K., 2012a. A thermodynamic and kinetic study of the de- and rehydration of $Ca(OH)_2$ at high H_2O partial pressures for thermo-chemical heat storage. Thermochim. Acta 538, 9–20.
Schaube, F., Kohzer, A., Schütz, J., Wörner, A., Müller-Steinhagen, K., 2012b. De- and rehydration of Ca(OH)2 in a reactor with direct heat transfer for thermo-chemical heat storage. Part A: Experimental results. Chem. Eng. Res. Des. 538, 9–20.
Schmidt, M., Szczukowski, C., Roßkopf, C., Linder, M., Wörner, A., 2014. Experimental results of a 10 kW high temperature thermochemical storage reactor based on calcium hydroxide. Appl. Therm. Eng. 62, 553–559.
Villermaux, J., 1979. Les réacteurs chimiques solaires. Entropie 85, 25–31.
Wentworth, W.E., Chen, E., 1976. Simple thermal decomposition reactions for storage of solar thermal energy. Sol. Energy 18, 205–214.
Werekobrobby, C.Y., 1980. Calcium hydroxide storage for solar thermal power generation systems. Colloque: le génie chimique et le stockage de l'énergie 8 & 9 December, (4-1)–(4-5).
Wong, B., Brown, L., Schaube, F., Tamme, R., Sattler, C., 2010. Oxide Based Thermochemical Heat Storage. SolarPACES, Perpignan, France, pp. 21–24.